ERCC1/XPF Removes the 3′ Overhang from Uncapped Telomeres and Represses Formation of Telomeric DNA-Containing Double Minute Chromosomes

Xu-Dong Zhu,[1,4] Laura Niedernhofer,[2,5]
Bernhard Kuster,[3,6] Matthias Mann,[3]
Jan H.J. Hoeijmakers,[2] and Titia de Lange[1,*]
[1]The Rockefeller University
New York, New York 10021
[2]MGC-Department of Cell Biology & Genetics
Centre for Biomedical Genetics
Erasmus Medical Center
3000 DR Rotterdam
The Netherlands
[3]Protein Interaction Laboratory
University of Southern Denmark
DK-5230 Odense
Denmark

Summary

Human telomeres are protected by TRF2. Inhibition of this telomeric protein results in partial loss of the telomeric 3′ overhang and chromosome end fusions formed through nonhomologous end-joining (NHEJ). Here we report that ERCC1/XPF-deficient cells retained the telomeric overhang after TRF2 inhibition, identifying this nucleotide excision repair endonuclease as the culprit in overhang removal. Furthermore, these cells did not accumulate telomere fusions, suggesting that overhang processing is a prerequisite for NHEJ of telomeres. ERCC1/XPF was also identified as a component of the telomeric TRF2 complex. ERCC1/XPF-deficient mouse cells had a novel telomere phenotype, characterized by Telomeric DNA-containing Double Minute chromosomes (TDMs). We speculate that TDMs are formed through the recombination of telomeres with interstitial telomere-related sequences and that ERCC1/XPF functions to repress this process. Collectively, these data reveal an unanticipated involvement of the ERCC1/XPF NER endonuclease in the regulation of telomere integrity and establish that TRF2 prevents NHEJ at telomeres through protection of the telomeric overhang from ERCC1/XPF.

Introduction

Mammalian telomeres are composed of TTAGGG repeat arrays and associated proteins that function to protect and maintain the telomeric DNA. Telomere protection depends on TRF2, a small dimeric protein that binds along the duplex telomeric repeat tract (Bilaud et al., 1997; Broccoli et al., 1997; reviewed in de Lange, 2002). Inhibition of TRF2 with a dominant-negative allele (TRF2$^{\Delta B\Delta M}$) or RNAi results in immediate deprotection of

*Correspondence: delange@rockefeller.edu
[4]Present address: Department of Biology, McMaster University, Hamilton, Ontario, Canada.
[5]Present address: Department of Molecular Genetics and Biochemistry, University of Pittsburgh, Pittsburgh, PA.
[6]Present address: Cellzome AG, Meyerhofstrasse 1, 69117 Heidelberg, Germany.

telomeres (Takai et al., 2003; van Steensel et al., 1998). Such uncapped telomeres activate a DNA damage response, leading to the binding of DNA damage response factors to chromosome ends and the induction of apoptosis or senescence (Karlseder et al., 1999; Smogorzewska and de Lange, 2002; Takai et al., 2003; van Steensel et al., 1998). The uncapped telomeres are processed by nonhomologous end joining (NHEJ), resulting in telomere-telomere fusion and formation of dicentric and multicentric chromosomes (Bailey et al., 2001; Smogorzewska et al., 2002; van Steensel et al., 1998). The consequences of TRF2 inhibition are indistinguishable from the events following replicative telomere shortening (Smogorzewska and de Lange, 2002), suggesting that telomeres lacking sufficient TRF2 resemble critically shortened telomeres. In agreement, overexpression of TRF2 can protect very short telomeres from fusion and delays the onset of senescence (Karlseder et al., 2002).

A major challenge is to determine what change in the structure of shortened telomeres renders them nonfunctional and what type of signal alerts cells to this change. One possibility is that cells respond when one or more telomeres have lost the telomeric DNA altogether (Baird et al., 2003). However, the fact that TRF2 inhibition can induce a DNA damage response without detectable loss of the double-stranded DNA argues that the signal can also involve a change in the state of the telomere rather than its complete disappearance (Karlseder et al., 1999; Takai et al., 2003; van Steensel et al., 1998).

Absence of the 3′ telomeric overhang was recently proposed to be the altered telomere state that induces cells to arrest (Stewart et al., 2003). Human telomeres carry several hundred nucleotides of TTAGGG repeats at their termini (Makarov et al., 1997), and this part of the telomere may be crucial for telomere protection. Consistent with this view, the (partial) loss of the 3′ overhang is an early sign of telomere deprotection after TRF2 inhibition (van Steensel et al., 1998).

A second, possibly related, change in telomere state could be the opening of t loops. T loops are large duplex loops formed through the strand invasion of the single-stranded telomeric overhang (Griffith et al., 1999). In vitro, TRF2 has the ability to promote t loop formation, suggesting that t loops may be part of the protection afforded by TRF2 (Stansel et al., 2001). In the t loop, the 3′ overhang is tucked into the duplex part of the telomere, and this may be sufficient to protect the overhang from degradation and prevent telomere fusion by NHEJ. Thus, loss of telomeric overhangs may be a consequence (or a cause) of t loop resolution when telomeres have become very short or when TRF2 function is impaired.

The greatest overhang loss (∼50% reduction in the ss TTAGGG repeat signal) is observed in a setting that allows cells to undergo several divisions after TRF2 inhibition (van Steensel et al., 1998). This observation raised the possibility that the overhangs disappear as a consequence of DNA replication. If overhangs are not actively created at the end generated by leading strand DNA

A

B

C

Effect of XPF status on TRF2$^{\Delta B \Delta M}$-induced anaphase bridges (100 anaphase cells)

Cell line/retrovirus	XPF	% cells with lagging chromosomes	% cells with chromatin bridges
IMR90-LT/vector	+	24	4
IMR90-LT/TRF2$^{\Delta B \Delta M}$	+	20	56
GM08437B/vector	-	34	16
GM08437B/TRF2$^{\Delta B \Delta M}$	-	28	26
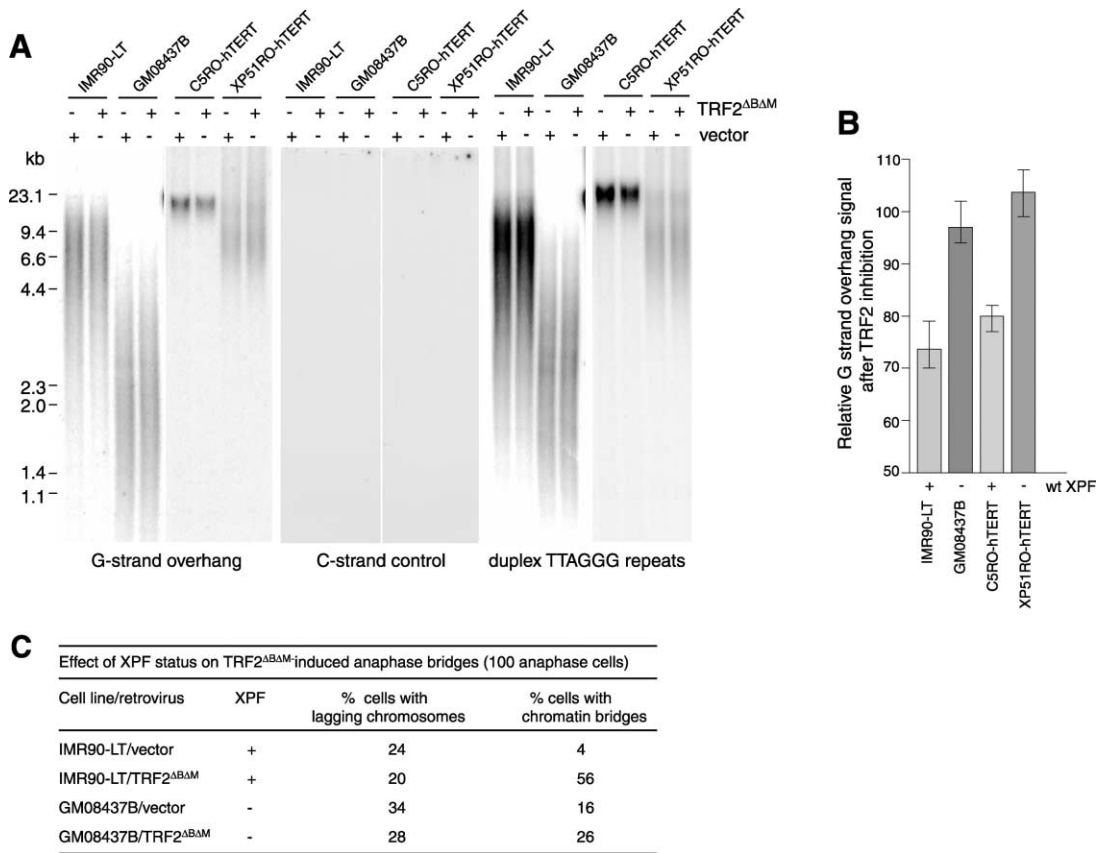
Figure 1. Diminished G-Strand Overhang Loss in XPF-Deficient Human Cells Expressing TRF2$^{\Delta B \Delta M}$

(A) Analysis of G-strand overhangs and telomere length. GM08437B and XP51RO-hTERT cells (from XPF patients) were infected with vector or TRF2$^{\Delta B \Delta M}$ viruses and, after 10 days, DNA was separated on 0.7% agarose gel. IMR90-LT and C5RO-hTERT cells (both XPF proficient) were processed in parallel as controls. Gels were first hybridized with an end-labeled (CCCTAA)$_4$ probe under native conditions to detect the 3′ G-strand overhangs or with a (TTAGGG)$_4$ probe as a C-strand control. After quantification, the DNA was alkali-denatured in situ and rehybridized with the same probe to detect duplex telomeric DNA. MW markers are indicated on the left.

(B) Quantitation of relative loss of G-strand overhang signal from three independent experiments. G-strand overhang signal for each DNA sample was normalized to the signal of duplex of TTAGGG repeats determined in the same gel. The plots give the ratio (in percentage) of the normalized overhang signal in cells expressing TRF2$^{\Delta B \Delta M}$ to the normalized overhang signal in vector control cells. The plot represents the percentage loss of G-strand overhang signal after TRF2 inhibition. Standard deviations derived from three independent experiments are indicated.

(C) Occurrence of anaphase bridges and lagging chromosomes in IMR90-LT and GM08437B infected with TRF2$^{\Delta B \Delta M}$ or vector control. Anaphases were examined 10 days after infection using DAPI-stained cells.

synthesis, the overhang signal will diminish gradually with cell divisions, as was observed (van Steensel et al., 1998). However, overhang loss (albeit more modest) was also noted in cells that had sustained TRF2 inhibition but did not progress through S phase (Smogorzewska et al., 2002). This would suggest that there is an active nuclease at work. Here we identify ERCC1/XPF as this nuclease.

ERCC1 and XPF form a complex that functions as a structure-specific endonuclease. This complex cleaves on the 5′ side of bubble structures containing damaged DNA (Aboussekhra et al., 1995; Park and Sancar, 1994; reviewed in de Laat et al., 1999; Hoeijmakers, 2001). ERCC1/XPF also cuts DNA duplexes adjacent to a 3′ single-stranded DNA flap (de Laat et al., 1998a, 1998b). Patients with hypomorphic mutations in XPF are sensitive to UV, develop skin cancer, and have other symptoms of xeroderma pigmentosa (Brookman et al., 1996;

Kondo et al., 1989; Sijbers et al., 1996). Although mutations in ERCC1 are not found in the human population, mouse cells lacking ERCC1 function are also UV sensitive (McWhir et al., 1993; Weeda et al., 1997). In addition, the ERCC1/XPF endonuclease and its yeast homolog Rad1/Rad10 play a role in processing intermediates in homologous recombination (Adair et al., 2000; Fishman-Lobell and Haber, 1992; Ivanov and Haber, 1995; Niedernhofer et al., 2001; Sargent et al., 2000; Schiestl and Prakash, 1988).

Here we show that ERCC1/XPF associates with TRF2 and is present at telomeres. Our data indicate that ERCC1/XPF-deficient cells retain the telomeric overhang after TRF2 inhibition, identifying this complex as the culpable nuclease in overhang processing. The persistence of the overhang was accompanied by a lack of telomere fusions, suggesting that the overhang per se is sufficient to prevent telomere fusion, even when

A

ERCC1$^{+/+}$/TRF2$^{\Delta B\Delta M}$ XPC$^{-/-}$/TRF2$^{\Delta B\Delta M}$ ERCC1$^{-/-}$/vector ERCC1$^{-/-}$/TRF2$^{\Delta B\Delta M}$

B

C

Chromosomal abnormalities in 50 metaphase cells

Genotype/ Retrovirus	Breaks	Fusions without telomeric signals	Fusions with telomeric signals	Fraction of cells with telomere fusions
ERCC1$^{+/+}$/vector	4; 4	2; 0	0; 0	0%; 0%
XPC$^{-/-}$/vector	3; 4	9; 11	0; 0	0%; 0%
ERCC1$^{-/-}$/vector	4; 4	8; 10	0; 0	0%; 0%
ERCC1$^{+/+}$/TRF2$^{\Delta B\Delta M}$	2; 4	2; 2	30; 27	38%; 34%
XPC$^{-/-}$/TRF2$^{\Delta B\Delta M}$	3; 5	10; 11	28; 28	36%; 36%
ERCC1$^{-/-}$/TRF2$^{\Delta B\Delta M}$	8; 12	10; 13	2; 3	4%; 4%

Figure 2. Absence of Telomere Fusions in ERCC1$^{-/-}$ MEFs Expressing TRF2$^{\Delta B\Delta M}$

(A) Metaphase spreads from ERCC1$^{+/+}$ and XPC$^{-/-}$ MEFs expressing TRF2$^{\Delta B\Delta M}$ and ERCC1$^{-/-}$ expressing either vector or TRF2$^{\Delta B\Delta M}$. Chromosomes were stained with DAPI and false-colored in red. Telomeric DNA was detected by FISH with a FITC-conjugated (CCCTAA)$_3$-containing PNA probe (green). White arrows indicate telomere end-to-end fusions. Enlarged images are shown below.
(B) Western analysis verifying equal expression of TRF2$^{\Delta B\Delta M}$ in the infected MEFs. Forty micrograms fractionated WCE protein was probed with anti-TRF2 (Ab#647).
(C) Summary of chromosomal abnormalities in ERCC1$^{+/+}$, ERCC1$^{-/-}$, and XPC$^{-/-}$ MEFs expressing either vector or TRF2$^{\Delta B\Delta M}$. The numbers are derived from two independent experiments.

TRF2 is inhibited. We also identify a role for ERCC1/XPF in protecting telomeres from recombining with chromosome internal sites.

Results and Discussion

No G-Strand Overhang Loss in XPF-Deficient Cells

As ERCC1/XPF can cleave next to a 3′ single-strand protrusion in vitro (de Laat et al., 1998a, 1998b), it has the potential to remove the G-strand overhang from telomeres. To determine whether ERCC1/XPF is the nuclease involved, we examined the fate of G-strand overhangs in XPF-deficient human cells with diminished TRF2 function. Two human cell lines with severely reduced XPF function are available. One is transformed with SV40 and the other is immortalized by hTERT (GM08437B and XP51RO-hTERT, respectively). Both were infected with a retrovirus expressing the TRF2$^{\Delta B\Delta M}$ dominant-negative allele of TRF2 or the pLPC retroviral vector. As a control, TRF2$^{\Delta B\Delta M}$ or the pLPC vector was introduced into IMR90 cells, transformed with SV40 large T antigen (IMR90-LT). HTERT-immortalized normal

human fibroblasts (C5RO-hTERT) served as a second control. Both control cells and XPF-deficient cells expressed similar levels of TRF2$^{\Delta B\Delta M}$ (data not shown). Consistent with published data, when forced to express TRF2$^{\Delta B\Delta M}$, the control cells showed a reduction of the G-strand overhang signal (Figures 1A and 5B). In contrast, cells lacking normal XPF function showed no significant change in the G-strand overhang signal after inhibition of TRF2 (Figures 1A and 1B). This indicates that ERCC1/XPF is the main nuclease that removes the G-strand overhangs from uncapped telomeres.

Absence of ERCC1/XPF Prevents Telomere Fusions

We next used ERCC1/XPF-deficient cells to ask whether the G-strand overhang is sufficient to prevent telomere fusions by NHEJ. Telomere fusions give rise to anaphase chromatin bridges that can be assessed in a quantitative manner (van Steensel et al., 1998). Inhibition of TRF2 in SV40 large T immortalized IMR90 cells, which have normal ERCC1/XPF function, resulted in up to 56% of the anaphase cells containing one or more chromatin bridge (Figure 1C). This value represents a 14-fold in-

crease in the fraction of cells with anaphase bridges compared to control cells. The XPF-deficient cells showed a high basal level of anaphase bridges (16% of the anaphase cells had one or more chromatin bridge), perhaps due to general genome instability in these cells. Inhibition of TRF2 increased the frequency of anaphase bridges somewhat but the increase was very modest, resulting in only 26% of the cells having one or more anaphase bridge. Thus, in contrast to XPF-proficient cultures showing a 14-fold increase in cells with anaphase bridges, XPF-deficient cells only showed a 1.6-fold higher frequency of anaphase bridges in response to TRF2 inhibition. As a control, TRF2 inhibition did not affect the occurrence of lagging chromosomes.

The role of ERCC1/XPF in facilitating NHEJ of uncapped telomeres was further corroborated by analysis of telomere fusions in ERCC1$^{-/-}$ mouse embryo fibroblasts (Weeda et al., 1997). Because the two components of this complex are codependent, cells lacking ERCC1 have reduced levels of XPF and vice versa (Biggerstaff et al., 1993; Houtsmuller et al., 1999; Sijbers et al., 1996; van Vuuren et al., 1993; Yagi et al., 1997). Immortalized ERCC1$^{-/-}$ MEFs and ERCC1-proficient control cells were infected with the TRF2 dominant-negative allele or a control retrovirus and then processed for telomeric FISH on metaphase spreads (Figure 2A). The level of TRF2$^{\Delta B \Delta M}$ expression in ERCC1$^{-/-}$ MEFs was similar to that in ERCC1$^{+/+}$ and XPC$^{-/-}$ MEFs (Figure 2B). As expected, inhibition of TRF2 in wild-type control cells or XPC-deficient cells gave rise to numerous chromosome end fusions with telomeric signals at the fusion site. In these settings, approximately 30%–40% of the metaphases contain one or more telomere fusion event (Figures 2A and 2C). In contrast, ERCC1$^{-/-}$ MEFs, when forced to express TRF2$^{\Delta B \Delta M}$, did not accumulate telomere fusions (Figure 2A) and contained only 2 or 3 telomere fusions in 50 metaphase cells, which is at least 9-fold fewer than in wild-type counterpart (Figure 2C). Both ERCC1$^{-/-}$ and XPC$^{-/-}$ contained a low level of dicentric chromosomes that were not due to telomere fusions and were not affected by TRF2 inhibition (Figure 2C). These dicentric chromosomes are mostly likely due to genomic instability as a result of the defect in the NER pathway. These chromosomal abnormalities correlate with the higher background of anaphase bridges in XPF-deficient human cells (Figure 1C), further suggesting that these cells suffer from genomic instability due to a defect in NER. Taken together, these results show that ERCC1/XPF are required for the removal of the G-strand overhangs and for the fusion of uncapped telomeres.

Telomere fusions are generated by DNA ligase IV-dependent NHEJ (Figure 3) (Smogorzewska et al., 2002). We had previously speculated that this pathway would require the removal of the telomeric overhang, and preliminary evidence had suggested that G-strand overhang removal was an active process, implicating a nuclease (Smogorzewska et al., 2002). Since deficiency in ERCC1/XPF results in overhang persistence and also blocks telomere fusion, these data corroborate the previously proposed scenario for telomere fusion. We imagine that upon TRF2 inhibition telomeres unfold, leading to exposure of the 3' end. Cleavage by ERCC1/XPF would remove the single-stranded overhang, creating the substrate for DNA ligase IV-mediated NHEJ (Figure
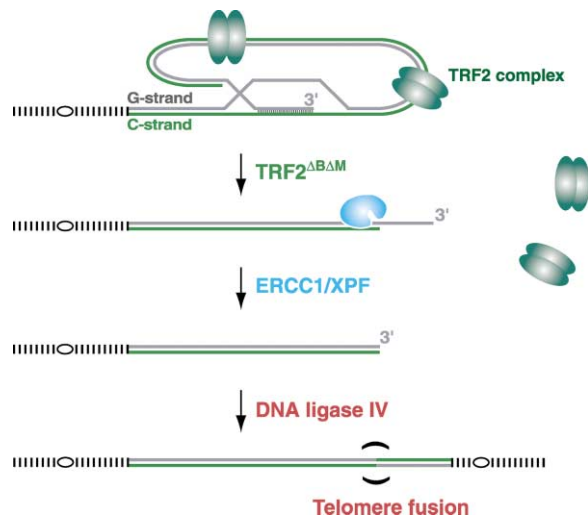
Figure 3. Model for Telomere Processing after Experimental Uncapping

Inhibition of TRF2 due to TRF2$^{\Delta B \Delta M}$ expression is proposed to result in the opening of the t loop or failure to reform the t loop after DNA replication, leading to the exposure of 3' G-strand overhang. ERCC1/XPF cleaves the 3' overhang, generating a substrate for NHEJ by DNA ligase IV. The product of the ligation is a dicentric chromosome formed through the covalent fusion of two telomeres. The ERCC1/XPF involved in cleaving the 3' overhang could be either recruited to the telomere by residual TRF2 or it could originate from the large nucleoplasmic pool of ERCC1/XPF.

3). The finding that uncapped telomeres are protected from NHEJ when their overhangs persist further underscores the importance of this part of the telomere. It also reveals that, with regard to NHEJ, the main protective role of TRF2 is to prevent overhang loss. The mechanism by which TRF2 blocks ERCC1/XPF from removing the 3' overhang will require further testing.

ERCC1/XPF in the Telomeric TRF2 Complex
Unexpectedly, ERCC1/XPF was also found to be a component of the telomeric protein complex. A TRF2 complex isolated by immunoprecipitation from heparin-sepharose fractionated HeLa nuclear extract was previously shown to contain the Rad50 component of the Mre11 complex and the TRF2 interacting factor hRap1 (Zhu et al., 2000). The same TRF2 complex contained a weak band migrating at 110 kDa (Figure 4A) which was absent from control IPs with preimmune serum (data not shown). Nanoelectrospray tandem mass spectrometry (Wilm et al., 1996) of three tryptic peptides derived from the 110 kDa band identified XPF (Figure 4B). This interaction was verified with two unrelated TRF2 sera (#647 and #508) which both precipitated XPF and its partner ERCC1 (Figure 4C). As a negative control, TRF1 and tankyrase 1 were not brought down in the TRF2 immunoprecipitates (Zhu et al., 2000; data not shown). Immunoprecipitates with XPF and ERCC1 sera contained TRF2 (Figure 4D), and the association was verified in primary human fibroblasts (Figure 4E). Other abundant nucleotide excision repair proteins such as XPA, XPC, and XPG did not interact with TRF2 (Figure 4C, data not shown). We estimate that the fraction of the ERCC1/
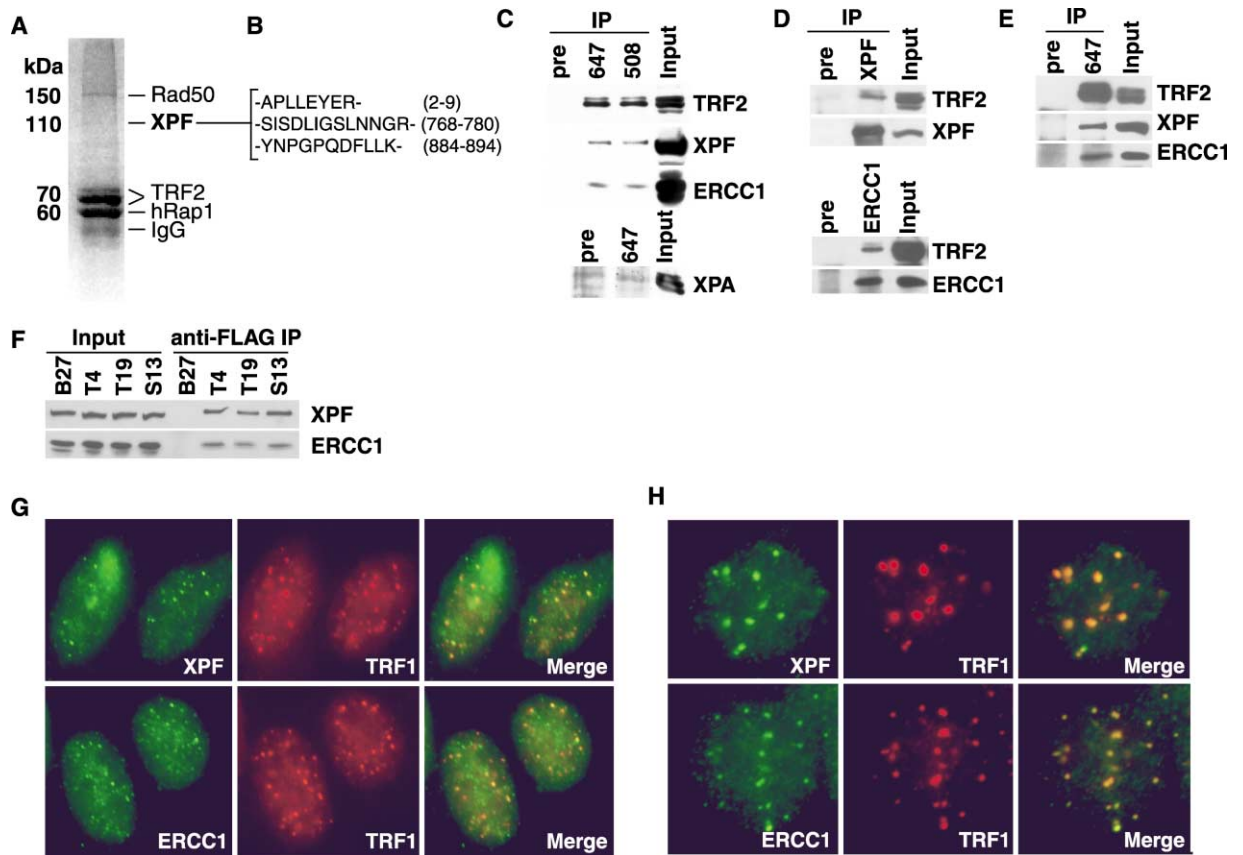
Figure 4. ERCC1/XPF in the Telomeric TRF2 Complex

(A) Identification of TRF2 associated proteins. Five bands that were consistently observed are indicated. Bands corresponding to Rad50, TRF2, and hRap1 have been reported previously in Zhu et al. (2000).

(B) Identification of XPF by nanoelectrospray tandem mass spectrometry. Sequencing of three tryptic peptides unambiguously identified the presence of human XPF in the 110 kDa band. The position of each peptide is given.

(C) Co-IP of ERCC1/XPF with TRF2. IPs with HeLa nuclear extract using either preimmune serum or anti-TRF2 antibodies (Ab#647 or Ab#508). Western blot analysis was performed with rabbit anti-XPF, anti-ERCC1, anti-XPA, and anti-TRF2 (Ab#647) sera. Input: 11% of material used for IPs.

(D) Co-IP of TRF2 with ERCC1/XPF. IPs as in (C) but with anti-XPF and anti-ERCC1 antibodies. Western blot analysis was carried out with rabbit anti-TRF2 (Ab#647), anti-XPF, and anti-ERCC1 sera. For the TRF2 input, 6% was loaded; for the XPF input, 2% was loaded; for the ERCC1 IPs, 10% of the input was loaded.

(E) Co-IP of ERCC1/XPF with TRF2 from IMR90 cells. IP as in (C) except whole-cell extract from young IMR90 cells was used. Input represents 2%.

(F) DNA binding activity of TRF2 was not required for association with the ERCC1/XPF complex. IPs were done with FLAG antibody M2 and whole-cell extracts from HTC75-derived cell lines (van Steensel et al., 1998) induced to express FLAG-tagged TRF2$^{\Delta B \Delta M}$ (T4 and T19), FLAG-tagged TRF2$^{\Delta B}$ (S13), or no exogenous protein (B27). Western blot analysis was performed with rabbit anti-XPF and anti-ERCC1. Input represents 2%.

(G) Colocalization of XPF and ERCC1 with TRF1 at HeLa telomeres. HeLaI.2.11 cells were detergent-extracted, fixed, permeabilized, and immunostained with mouse anti-TRF1 antibody (TRITC) in conjunction with rabbit anti-XPF and anti-ERCC1 (FITC) as indicated. Two nuclei are shown in each panel.

(H) Colocalization of XPF and ERCC1 proteins with TRF1 in a subset of cells of the ALT cell line WI38VA13/2RA. Interphase cells were extracted with detergent and stained with the indicated antibodies as described above. A single nucleus is shown in both cases.

XPF associated with TRF2 is relatively small (~1% of HeLa XPF was recovered with TRF2; Figure 4C and data not shown), and only a minor fraction of TRF2 seemed to be associated with XPF (Figure 4D). The finding that most ERCC1/XPF is not associated with TRF2 (or telomeres) is consistent with photobleaching experiments demonstrating that the majority of ERCC1/XPF migrates as a separate entity throughout the nucleus (Houtsmuller et al., 1999).

To verify that the association of ERCC1/XPF with TRF2 was not mediated by DNA tethering, we analyzed this interaction using a tagged TRF2 deletion mutant lacking the DNA binding domain (TRF2$^{\Delta B \Delta M}$) in parallel with a mutant of TRF2 that is DNA binding competent (TRF2$^{\Delta B}$) (van Steensel et al., 1998). Immunoprecipitates of both versions of TRF2 using an antibody against the tag contained ERCC1/XPF (Figure 4F), indicating that DNA binding by TRF2 is not required for the interaction. In agreement, the interaction was resistant to 500 mM KCl (data not shown), a condition that abolishes the DNA binding activity of TRF2.

To examine whether XPF and ERCC1 are associated with telomeres, we carried out dual indirect immunofluorescence (IF) with antibodies to TRF1 (as a marker for

telomeres [Chong et al., 1995; van Steensel and de Lange, 1997]) and antibodies to XPF or ERCC1. As XPF and ERCC1 show dispersed nuclear signals potentially masking their presence at telomeres, we extracted nucleoplasmic proteins with mild detergent prior to IF (Zhu et al., 2000). After this treatment, XPF and ERCC1 showed a pattern of discrete punctate signals, a subset of which colocalized with TRF1 (Figure 4G). Control experiments omitting either the ERCC1/XPF antibodies or TRF1 antibody showed that there was no bleed-through from FITC channel to TRITC channel or vice versa (data not shown). Colocalization of ERCC1/XPF with TRF1 was also observed in a second cell line (WI38VA13/2RA), which maintains its telomeres through a telomerase-independent mechanism. In a subset of these cells, telomeres form large foci containing telomeric DNA, telomeric proteins, and a large number of other factors. ERCC1/XPF colocalized with these elements (Figure 4H).

ERCC1$^{-/-}$ MEFs Generate Telomeric DNA-Containing Double Minute Chromosomes

Since ERCC1/XPF is present at telomeres, we asked whether the absence of this complex affects telomere structure and function. The effect of ERCC1/XPF on the structure of the telomeric DNA was examined using three independent litters from crosses of ERCC$^{+/-}$ mice. Genomic blotting of the DNA from fibroblasts derived from littermate embryos showed the expected variability of telomeric restriction fragments but no consistent length change associated with the ERCC1$^{-/-}$ genotype (Figure 5A). Furthermore, ERCC1$^{-/-}$ MEFs had single-stranded telomeric overhangs as detected by annealing of a C-strand oligonucleotide to telomeric termini (Figure 5B). The G-strand signal was derived from 3′ overhangs since it was sensitive to digestion with exonuclease I (data not shown). Consistent with the integrity of their telomeric DNA, ERCC1$^{-/-}$ MEFs did not show chromosome end-to-end fusions in metaphase (Figures 2A and 2C).

Fluorescence in situ hybridization (FISH) with a telomeric probe revealed the presence of several extrachromosomal telomeric signals in metaphase spreads of immortalized ERCC1$^{-/-}$ MEFs (Figure 6). Most of the extrachromosomal telomeric signals formed two dots, and the signal intensity of these dots was comparable to the telomeric signals on the intact chromosomes. DAPI staining showed that these elements contained substantial amounts of nontelomeric DNA. The size of the elements appeared to vary substantially and, in some cases, the elements contained centromeric heterochromatin (one example in Figure 6). These extrachromosomal elements resembled Double Minute chromosomes (DMs), which are circular extrachromosomal elements, appearing as two closely positioned dots in metaphase. DMs were identified in multidrug resistance cancer cells and certain other mammalian cells with amplified DNA (Hahn, 1993). We refer to the extrachromosomal elements in the ERCC$^{-/-}$ cells as Telomeric DNA-containing Double Minutes (TDMs) to distinguish them from other DMs which do not contain telomeric DNA (Lin et al., 1990).

The frequency of TDMs was determined by telomeric FISH analysis of a series of ERCC1-proficient and
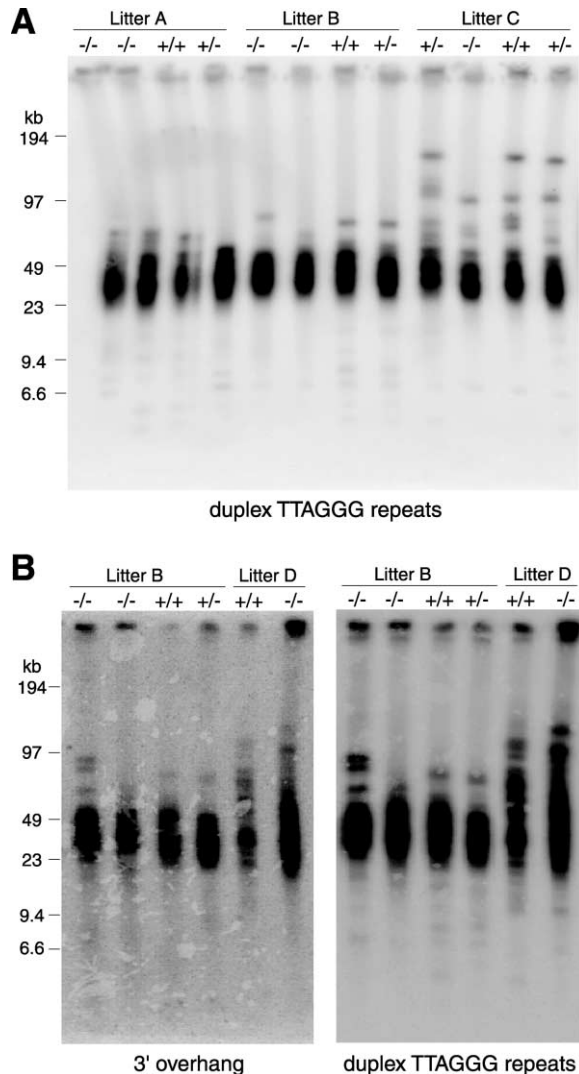
Figure 5. Telomere Structure of ERCC1$^{-/-}$ MEFs

(A) Duplex TTAGGG repeats from early passage of primary MEFs. Twelve AluI/MboI-digested DNA plugs derived from three litters (genotypes indicated) were separated on a CHEF gel. Hybridization was carried out in-gel with an end-labeled (CCCTAA)$_4$ olignucleotide after in situ denaturation of the DNA. Molecular weight markers are indicated on the left.

(B) Analysis of G-strand overhangs and telomere length from immortalized MEFs. Four primary MEFs from litter B were immortalized by 3T3 protocol, and two primary MEFs from litter D were spontaneously immortalized and AluI/MboI-digested DNA plugs were separated on a CHEF gel. Hybridization was first carried out in-gel under native conditions with an end-labeled (CCCTAA)$_4$ oligonucleotide to detect the 3′ G-strand overhangs. The same gel was then alkali-denatured and hybridized to the same probe to detect duplex telomeric DNA. Genotypes are indicated above the lane and the molecular weights of DNA markers are shown on the left.

ERCC1-deficient MEFs derived from different crosses. The MEFs were either immortalized spontaneously, processed according to a 3T3 protocol, or transformed with SV40 large T antigen. TDMs were observed rarely in cells wild-type or cells heterozygous for ERCC1 (0.04–0.2 TDMs per metaphase) (Figure 6B). In contrast, immortalized ERCC1$^{-/-}$ MEFs had a 10-fold higher fre-

A
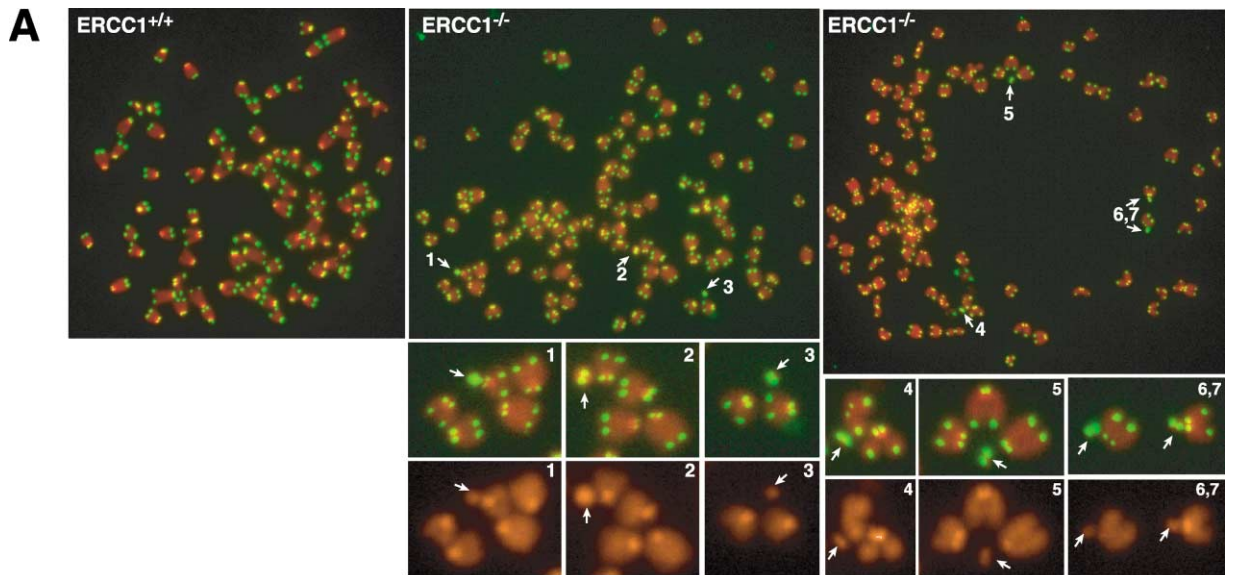
B

Frequency of TDMs formation

Cell line	Litter	Immortalization	Number of cells examined	Fraction of cells with TDMs	Number of TDMs per cell
ERCC1$^{+/+}$	B	SV40 large T	50	14%	0.18
ERCC1$^{+/-}$	B	SV40 large T	50	14%	0.18
ERCC1$^{+/+}$	B	3T3	50	6%	0.06
ERCC1$^{+/-}$	B	3T3	50	4%	0.04
ERCC1$^{+/+}$	D	spontaneous	50	16%	0.20
ERCC1$^{-/-}$-I	B	SV40-large T	50	52%	1.80
ERCC1$^{-/-}$-II	B	SV40-large T	50	44%	1.62
ERCC1$^{-/-}$-I	B	3T3	50	68%	1.46
ERCC1$^{-/-}$-II	B	3T3	50	48%	1.20
ERCC1$^{-/-}$	D	spontaneous	50	86%	3.10
XPC$^{-/-}$		spontaneous	100	4%	0.04

Figure 6. Identification of Telomeric DNA-Containing Double Minute Chromosomes in ERCC1 Null Cells

(A) Metaphase spreads from ERCC1$^{+/+}$ MEFs and ERCC1$^{-/-}$ MEFs. Chromosomes were stained with DAPI and false-colored in red. Telomeric DNA was detected by FISH with a FITC-conjugated (CCCTAA)$_3$-containing PNA probe (green). White arrows indicate TDMs. Enlarged images of seven TDMs are shown below with (top) and without (bottom) the telomeric FISH signal. One of the TDMs (#2) contains a segment of more intense DAPI stain indicative of the presence of centric heterochromatin.

(B) Summary of TDM frequencies in immortalized MEFs of different genotypes.

quency of TDMs (1.2–3.1 TDMs per metaphase) (Figure 6B). As a control for the effects of NER deficiency, immortalized XPC$^{-/-}$ MEFs were examined and found to have wild-type levels of TDMs. These results indicated that TDMs are not due to NER deficiency per se, but specific for the absence of ERCC1/XPF. In tumor cell lines, the selection for high expression levels of genes carried on DMs is thought to be responsible for their amplification. The copy number of TDMs is low in comparison, suggesting that they do not confer a selective advantage to the cells.

We propose that TDMs are formed through a recombination event between the telomere and chromosome-internal TTAGGG-like sequences. The genome of many vertebrates contain sequences that are closely related to telomeric repeats (Meyne et al., 1990). For instance,

the sequence 5′-TTAGGG-3′ is the consensus of the guinea-pig α-satellite repeat, one of the first mammalian DNA sequences to be determined (Southern, 1970). Although interstitial telomere-related sequences are pervasive, their sequences often diverge considerably from the telomeric DNA, and long stretches of exact TTAGGG repeats are rare (Fanning, 1987). We speculate that these chromosome internal telomere related loci can recombine with genuine telomeres. The product of such a recombination would be a terminally deleted chromosome and a circular product, the TDMs that we observe (Figure 7). We further propose that ERCC1/XPF can protect against this recombination event by cleaving an intermediate step. The ability of this endonuclease to cleave recombination intermediates has been documented in yeast and mammalian cells (Adair et al., 2000;
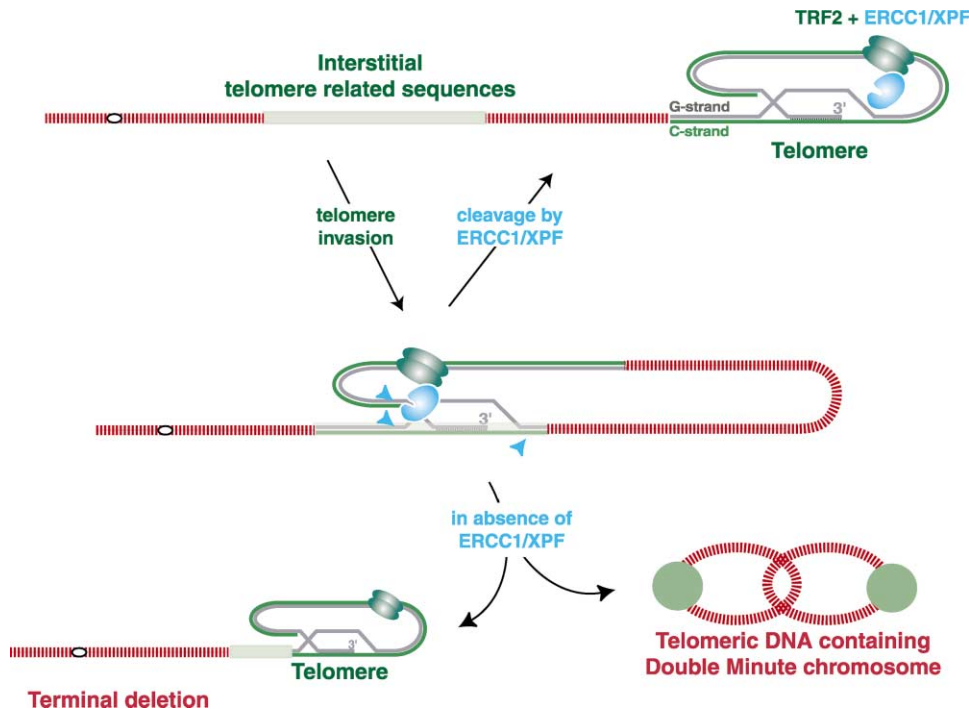
Figure 7. Model for the Role of ERCC1/XPF in Preventing Recombination between Telomeres and Interstitial Telomeric Sequences

ERCC1/XPF (blue arrow heads) is proposed to cleave inappropriate strand-invasion events of telomeres into interstitial telomere-related sequences. For instance, cleavage of the 3′ overhang would result in release of the strand-invasion event, and regeneration of the 3′ overhang (by telomerase or a nuclease) could reconstitute a functional telomere. In absence of ERCC1/XPF function, recombination between the telomere and the interstitial telomeric DNA results in a terminally deleted chromosome with a short telomere and a circular product containing telomeric DNA. After replication, the circular product will appear as a TDM in metaphase.

Fishman-Lobell and Haber, 1992; Ivanov and Haber, 1995; Niedernhofer et al., 2001; Sargent et al., 2000; Schiestl and Prakash, 1988). This speculative model raises the question of why ERCC1/XPF does not cleave the base of the t loop. Presumably, protection of the t loop must involve the inhibition of ERCC1/XPF at telomeres and the factor(s) involved in this regulation must be able to distinguish TTAGGG repeats from interstitial TTAGGG-related sequences.

Interestingly, ERCC1 null mice display other phenotypes that are not seen in mice with a defect in other NER components (de Vries et al., 1995; McWhir et al., 1993; Nakane et al., 1995; Sands et al., 1995; Weeda et al., 1997). For example, ERCC1 knockout mice display growth retardation and die before they are weaned. Furthermore, unlike MEFs derived from other NER-deficient mice, ERCC1 null MEFs undergo premature senescence. Our findings raise the possibility that TDM formation and presumed terminal deletions associated with TDMs could contribute to these phenotypes. A similar risk may also exist for patients with XPF deficiency, although interstitial telomere related sequences are less frequent in the human genome compared to some other vertebrates (Azzalin et al., 1997; Meyne et al., 1990), possibly lowering the frequency of recombination of telomeres with chromosome internal sites.

Experimental Procedures

Protein Extracts and Isolation of TRF2 Complex
Nuclear and whole-cell extracts were prepared as described in Zhu et al. (2000). In brief, nuclear extracts were made on ice by extraction of nuclei with 0.42 M KCl in buffer C (20 mM HEPES-KOH [pH 7.9], 25% glycerol, 0.1 mM EDTA, 5 mM MgCl$_2$, 1 mM dithiothreitol (DTT), 1 μg/ml aprotinin, 1 μg/ml leupeptin, 1 μg/ml pepstatin, and 0.5 mM phenylmethysulfonyl fluoride [PMSF]). Whole-cell extracts were made by resuspending cell pellets in 0.42 M KCl buffer C containing 0.2% Nonidet P-40. Extracts were then dialyzed at 4°C overnight against 100 mM KCl in buffer D (20 mM HEPES-KOH [pH 7.9], 20% glycerol, 0.2 mM EDTA, 0.2 mM EGTA, 1 mM DTT, and 0.5 mM PMSF) and stored at −80°C. Protein concentrations were determined using the Bradford assays (BioRad) with BSA as a standard.

TRF2 complex was isolated from HeLa nuclear extracts as described in Zhu et al. (2000). Proteins were visualized with Coomassie blue, and the band corresponding to 110 kDa was excised for mass spectrometric analysis as described in Zhu et al. (2000).

Cell Culture and Retroviral Infection
Cells were grown in DMEM medium with 10% fetal calf serum (for Phoenix cells, immortalized MEFs, and GM08347B [Coriell]), 15% FCS (for primary MEFs, C5RO-hTERT, XP51RO-hTERT, and IMR90), and 10% bovine calf serum (for HeLa and WI38VA13/2RA), supplemented with nonessential amino acids, glutamine, 100 U/ml penicillin, and 0.1 mg/ml streptomycin. Retroviral gene delivery was carried out as described in Karlseder et al. (2002). Phoenix ecotropic or amphotropic retroviral packaging cells were transfected with pLPC vector or pLPC containing TRF2$^{\Delta B,\Delta M}$ allele. At 24, 36, 48, and 60 hr posttransfection, the virus-containing medium was used to infect cells in the presence of polybrene (4 μg/ml). Twelve hours after the last infection, puromycin (2 μg/ml) was added to the medium and the cells were maintained in puromycin for 10 days.

Immunoblotting and Immunoprecipitation
Immunoblotting was carried out with HeLa nuclear extract (20 μg) or whole-cell extract (40 μg) as described in Zhu et al. (2000). Extracts were fractionated on 8% SDS-PAGE and transferred to nitrocellulose which was immunoblotted with monoclonal M2 anti-FLAG

antibody (Sigma) or rabbit anti-serum against TRF2 (Ab#647 and Ab#508; van Steensel et al., 1998; Zhu et al., 2000), XPF (Sijbers et al., 1996; van Vuuren et al., 1993), ERCC1 (Sijbers et al., 1996; van Vuuren et al., 1993), and XPA (Santa Cruz). Immunoprecipitation was performed with whole-cell extract (7 mg) and TRF2 preimmune serum, Ab#647, or M2 anti-FLAG antibody. Immunoprecipitates were fractionated on 8% SDS-PAGE, transferred to nitrocellulose, and immunoblotted as described.

Immunofluorescence

Immunofluorescence was performed essentially the same as described in Zhu et al. (2000). Cells were grown on coverslips, rinsed with PBS, and incubated in Triton X-100 buffer (0.5% Triton X-100, 20 mM HEPES-KOH [pH 7.9], 50 mM NaCl, 3 mM $MgCl_2$, and 300 mM sucrose) at room temperature for 5 min before fixation and permeabilization. For dual indirect immunofluorescence, fixed cells were blocked with 0.5% BSA (Sigma) and 0.2% gelatin (Sigma) in PBS and then incubated at room temperature for 2 hr with either mouse anti-TRF1 (1:5000) or mouse anti-TRF2 (1:1500) in conjunction with rabbit antiserum (1:200) against XPF and ERCC1. Following incubation, cells were washed in PBS and incubated with FITC-conjugated donkey anti-rabbit and TRITC-conjugated donkey anti-mouse antibodies (1:100 dilution; Jackson Laboratories) at room temperature for 1 hr. Cells were then washed and DNA was stained with 4, 6-diamidino-2-phenylindole (DAPI; 0.2 μg/ml). Images were then recorded on a Zeiss Axioplan microscope as described in Zhu et al. (2000).

Metaphase Chromosomal Spreads and FISH

Metaphase spreads were prepared essentially as described in van Steensel et al. (1998). Cells (∼80% confluence) were arrested in colcemide (0.1 μg/ml) for 60–90 min, harvested by trypsinization, incubated for 7 min at 37°C in 75 mM KCl, and fixed in freshly made methanol/glacial acidic acid (3:1). Cells were stored at 4°C, dropped onto wet slides, and air-dried overnight in a chemical hood.

Fluorescence in situ hybridization was performed according to Lansdorp et al. (1996). Slides with metaphase spreads were incubated with 0.5 μg/ml FITC-conjugated-(CCCTAA)₃ PNA probe (Applied Biosystems) for 2 hr at room temperature, washed, counterstained with 0.2 μg/ml DAPI, and embedded in 90% glycerol/10% PBS containing 1 mg/ml p-phenylene diamine (Sigma).

Preparation of DNA Plugs and Genomic DNA

MEFs at 1×10^7 cells/ml were mixed with an equal volume of 1% low melting point agarose (LMP) at 55°C and cast into 100 μl plug molds. After casting, plugs were incubated at 50°C in proteinase K-containing NDS buffer (0.5 M EDTA [pH 8.0]; 10 mM Tris-HCl [pH 8.0]; 1% N-lauryl sarkosyl) for 2 days. Plugs were then washed in TE at 4°C once for overnight, once for 2 hr, four times for 30 min each. Following preincubation in restriction buffer, plugs were digested with AluI and MboI at 37°C for overnight, equilibrated with 0.5xTBE buffer on ice for 30 min and loaded onto a 1% agarose gel in 0.5xTBE. Gels were run for 22 hr at 5.4 V/cm at a constant pulse time of 5 s using a CHEF DR-II pulsed-field apparatus (Bio-Rad). Genomic DNA from human cell lines was isolated and processed according to van Steensel and de Lange (1997). Following isolation, DNA was digested with AluI and MboI and loaded onto a 0.7% agarose gel in 0.5xTBE.

In-Gel G-Overhang Assay and Telomere Blots

In-gel G-overhang assay was done essentially the same as described in Hemann and Greider (1999). Following electrophoresis, gels were dried down at 40°C and prehybridzed at 50°C for 1 hr in Church mix (0.5 M Na_2HPO_4 [pH 7.2], 1 mM EDTA, 7% SDS, and 1% BSA), followed by hybridization at 50°C overnight with an end-labeled (CCCTAA)₄ or (TTAGGG)₄ oligonucleotide as described in Karlseder et al. (2002). After hybridization, gels were washed and exposed to Phosphoimager screens for overnight. Following G-overhang assay, gels were alkali denatured (0.5 M NaOH and 1.5 M NaCl), neutralized (3 M Nacl and 0.5 M Tris-HCl [pH 7.0]), rinsed with dH₂O, and reprobed with the (CCCTAA)₄ oligonucleotide (Hemann and Greider, 1999; Karlseder et al., 2002).

References

Aboussekhra, A., Biggerstaff, M., Shivji, M.K., Vilpo, J.A., Moncollin, V., Podust, V.N., Protic, M., Hubscher, U., Egly, J.M., and Wood, R.D. (1995). Mammalian DNA nucleotide excision repair reconstituted with purified protein components. Cell 80, 859–868.

Adair, G.M., Rolig, R.L., Moore-Faver, D., Zabelshansky, M., Wilson, J.H., and Nairn, R.S. (2000). Role of ERCC1 in removal of long nonhomologous tails during targeted homologous recombination. EMBO J. 19, 5552–5561.

Azzalin, C.M., Mucciolo, E., Bertoni, L., and Giulotto, E. (1997). Fluorescence in situ hybridization with a synthetic (T2AG3)n polynucleotide detects several intrachromosomal telomere-like repeats on human chromosomes. Cytogenet. Cell Genet. 78, 112–115.

Bailey, S.M., Cornforth, M.N., Kurimasa, A., Chen, D.J., and Goodwin, E.H. (2001). Strand-specific postreplicative processing of mammalian telomeres. Science 293, 2462–2465.

Baird, D.M., Rowson, J., Wynford-Thomas, D., and Kipling, D. (2003). Extensive allelic variation and ultrashort telomeres in senescent human cells. Nat. Genet. 33, 203–207.

Biggerstaff, M., Szymkowski, D.E., and Wood, R.D. (1993). Co-correction of the ERCC1, ERCC4 and xeroderma pigmentosum group F DNA repair defects in vitro. EMBO J. 12, 3685–3692.

Bilaud, T., Brun, C., Ancelin, K., Koering, C.E., Laroche, T., and Gilson, E. (1997). Telomeric localization of TRF2, a novel human telobox protein. Nat. Genet. 17, 236–239.

Broccoli, D., Smogorzewska, A., Chong, L., and de Lange, T. (1997). Human telomeres contain two distinct Myb-related proteins, TRF1 and TRF2. Nat. Genet. 17, 231–235.

Brookman, K.W., Lamerdin, J.E., Thelen, M.P., Hwang, M., Reardon, J.T., Sancar, A., Zhou, Z.Q., Walter, C.A., Parris, C.N., and Thompson, L.H. (1996). ERCC4 (XPF) encodes a human nucleotide excision repair protein with eukaryotic recombination homologs. Mol. Cell. Biol. 16, 6553–6562.

Chong, L., van Steensel, B., Broccoli, D., Erdjument-Bromage, H., Hanish, J., Tempst, P., and de Lange, T. (1995). A human telomeric protein. Science 270, 1663–1667.

de Laat, W.L., Appeldoorn, E., Jaspers, N.G., and Hoeijmakers, J.H. (1998a). DNA structural elements required for ERCC1-XPF endonuclease activity. J. Biol. Chem. 273, 7835–7842.

de Laat, W.L., Appeldoorn, E., Sugasawa, K., Weterings, E., Jaspers, N.G., and Hoeijmakers, J.H. (1998b). DNA-binding polarity of human replication protein A positions nucleases in nucleotide excision repair. Genes Dev. 12, 2598–2609.

de Laat, W.L., Jaspers, N.G., and Hoeijmakers, J.H. (1999). Molecular mechanism of nucleotide excision repair. Genes Dev. 13, 768–785.

de Lange, T. (2002). Protection of mammalian telomeres. Oncogene 21, 532–540.

de Vries, A., van Oostrom, C.T., Hofhuis, F.M., Dortant, P.M., Berg,

R.J., de Gruijl, F.R., Wester, P.W., van Kreijl, C.F., Capel, P.J., van Steeg, H., et al. (1995). Increased susceptibility to ultraviolet-B and carcinogens of mice lacking the DNA excision repair gene XPA. Nature *377*, 169–173.

Fanning, T.G. (1987). Origin and evolution of a major feline satellite DNA. J. Mol. Biol. *197*, 627–634.

Fishman-Lobell, J., and Haber, J.E. (1992). Removal of nonhomologous DNA ends in double-strand break recombination: the role of the yeast ultraviolet repair gene RAD1. Science *258*, 480–484.

Griffith, J.D., Comeau, L., Rosenfield, S., Stansel, R.M., Bianchi, A., Moss, H., and de Lange, T. (1999). Mammalian telomeres end in a large duplex loop. Cell *97*, 503–514.

Hahn, P.J. (1993). Molecular biology of double-minute chromosomes. Bioessays *15*, 477–484.

Hemann, M.T., and Greider, C.W. (1999). G-strand overhangs on telomeres in telomerase-deficient mouse cells. Nucleic Acids Res. *27*, 3964–3969.

Hoeijmakers, J.H. (2001). Genome maintenance mechanisms for preventing cancer. Nature *411*, 366–374.

Houtsmuller, A.B., Rademakers, S., Nigg, A.L., Hoogstraten, D., Hoeijmakers, J.H., and Vermeulen, W. (1999). Action of DNA repair endonuclease ERCC1/XPF in living cells. Science *284*, 958–961.

Ivanov, E.L., and Haber, J.E. (1995). RAD1 and RAD10, but not other excision repair genes, are required for double-strand break-induced recombination in *Saccharomyces cerevisiae*. Mol. Cell. Biol. *15*, 2245–2251.

Karlseder, J., Broccoli, D., Dai, Y., Hardy, S., and de Lange, T. (1999). p53- and ATM-dependent apoptosis induced by telomeres lacking TRF2. Science *283*, 1321–1325.

Karlseder, J., Smogorzewska, A., and de Lange, T. (2002). Senescence induced by altered telomere state, not telomere loss. Science *295*, 2446–2449.

Kondo, S., Mamada, A., Miyamoto, C., Keong, C.H., Satoh, Y., and Fujiwara, Y. (1989). Late onset of skin cancers in 2 xeroderma pigmentosum group F siblings and a review of 30 Japanese xeroderma pigmentosum patients in groups D, E and F. Photodermatol. *6*, 89–95.

Lansdorp, P.M., Verwoerd, N.P., van de Rijke, F.M., Dragowska, V., Little, M.T., Dirks, R.W., Raap, A.K., and Tanke, H.J. (1996). Heterogeneity in telomere length of human chromosomes. Hum. Mol. Genet. *5*, 685–691.

Lin, C.C., Meyne, J., Sasi, R., and Moyzis, R.K. (1990). Apparent lack of telomere sequences on double minute chromosomes. Cancer Genet. Cytogenet. *48*, 271–274.

Makarov, V.L., Hirose, Y., and Langmore, J.P. (1997). Long G tails at both ends of human chromosomes suggest a C strand degradation mechanism for telomere shortening. Cell *88*, 657–666.

McWhir, J., Selfridge, J., Harrison, D.J., Squires, S., and Melton, D.W. (1993). Mice with DNA repair gene (ERCC-1) deficiency have elevated levels of p53, liver nuclear abnormalities and die before weaning. Nat. Genet. *5*, 217–224.

Meyne, J., Baker, R.J., Hobart, H.H., Hsu, T.C., Ryder, O.A., Ward, O.G., Wiley, J.E., Wurster-Hill, D.H., Yates, T.L., and Moyzis, R.K. (1990). Distribution of non-telomeric sites of the (TTAGGG)n telomeric sequence in vertebrate chromosomes. Chromosoma *99*, 3–10.

Nakane, H., Takeuchi, S., Yuba, S., Saijo, M., Nakatsu, Y., Murai, H., Nakatsuru, Y., Ishikawa, T., Hirota, S., Kitamura, Y., et al. (1995). High incidence of ultraviolet-B-or chemical-carcinogen-induced skin tumours in mice lacking the xeroderma pigmentosum group A gene. Nature *377*, 165–168.

Niedernhofer, L.J., Essers, J., Weeda, G., Beverloo, B., de Wit, J., Muijtjens, M., Odijk, H., Hoeijmakers, J.H., and Kanaar, R. (2001). The structure-specific endonuclease Ercc1-Xpf is required for targeted gene replacement in embryonic stem cells. EMBO J. *20*, 6540–6549.

Park, C.H., and Sancar, A. (1994). Formation of a ternary complex by human XPA, ERCC1, and ERCC4(XPF) excision repair proteins. Proc. Natl. Acad. Sci. USA *91*, 5017–5021.

Sands, A.T., Abuin, A., Sanchez, A., Conti, C.J., and Bradley, A.

(1995). High susceptibility to ultraviolet-induced carcinogenesis in mice lacking XPC. Nature *377*, 162–165.

Sargent, R.G., Meservy, J.L., Perkins, B.D., Kilburn, A.E., Intody, Z., Adair, G.M., Nairn, R.S., and Wilson, J.H. (2000). Role of the nucleotide excision repair gene ERCC1 in formation of recombination-dependent rearrangements in mammalian cells. Nucleic Acids Res. *28*, 3771–3778.

Schiestl, R.H., and Prakash, S. (1988). RAD1, an excision repair gene of Saccharomyces cerevisiae, is also involved in recombination. Mol. Cell. Biol. *8*, 3619–3626.

Sijbers, A.M., de Laat, W.L., Ariza, R.R., Biggerstaff, M., Wei, Y.F., Moggs, J.G., Carter, K.C., Shell, B.K., Evans, E., de Jong, M.C., et al. (1996). Xeroderma pigmentosum group F caused by a defect in a structure-specific DNA repair endonuclease. Cell *86*, 811–822.

Smogorzewska, A., and de Lange, T. (2002). Different telomere damage signaling pathways in human and mouse cells. EMBO J. *21*, 4338–4348.

Smogorzewska, A., Karlseder, J., Holtgreve-Grez, H., Jauch, A., and de Lange, T. (2002). DNA ligase IV-dependent NHEJ of deprotected mammalian telomeres in G1 and G2. Curr. Biol. *12*, 1635–1644.

Southern, E.M. (1970). Base sequence and evolution of guinea-pig alpha-satellite DNA. Nature *227*, 794–798.

Stansel, R.M., de Lange, T., and Griffith, J.D. (2001). T-loop assembly in vitro involves binding of TRF2 near the 3′ telomeric overhang. EMBO J. *20*, E5532–E5540.

Stewart, S.A., Ben-Porath, I., Carey, V.J., O'Connor, B.F., Hahn, W.C., and Weinberg, R.A. (2003). Erosion of the telomeric single-strand overhang at replicative senescence. Nat. Genet. *33*, 492–496.

Takai, H., Smogorzewska, A., and d Lange, T. (2003). DNA damage foci at dysfunctional telomeres. Curr. Biol. *13*, 1540–1556.

van Steensel, B., and de Lange, T. (1997). Control of telomere length by the human telomeric protein TRF1. Nature *385*, 740–743.

van Steensel, B., Smogorzewska, A., and de Lange, T. (1998). TRF2 protects human telomeres from end-to-end fusions. Cell *92*, 401–413.

van Vuuren, A.J., Appeldoorn, E., Odijk, H., Yasui, A., Jaspers, N.G., Bootsma, D., and Hoeijmakers, J.H. (1993). Evidence for a repair enzyme complex involving ERCC1 and complementing activities of ERCC4, ERCC11 and xeroderma pigmentosum group F. EMBO J. *12*, 3693–3701.

Weeda, G., Donker, I., de Wit, J., Morreau, H., Janssens, R., Vissers, C.J., Nigg, A., van Steeg, H., Bootsma, D., and Hoeijmakers, J.H. (1997). Disruption of mouse ERCC1 results in a novel repair syndrome with growth failure, nuclear abnormalities and senescence. Curr. Biol. *7*, 427–439.

Wilm, M., Shevchenko, A., Houthaeve, T., Breit, S., Schweigerer, L., Fotsis, T., and Mann, M. (1996). Femtomole sequencing of proteins from polyacrylamide gels by nano-electrospray mass spectrometry. Nature *379*, 466–469.

Yagi, T., Wood, R.D., and Takebe, H. (1997). A low content of ERCC1 and a 120 kDa protein is a frequent feature of group F xeroderma pigmentosum fibroblast cells. Mutagenesis *12*, 41–44.

Zhu, X.D., Kuster, B., Mann, M., Petrini, J.H., and de Lange, T. (2000). Cell-cycle-regulated association of RAD50/MRE11/NBS1 with TRF2 and human telomeres. Nat. Genet. *25*, 347–352.